Molecular Biology of the Cell
Vol. 10, 4121–4133, December 1999

The Rho GTPase Rho3 Has a Direct Role in Exocytosis That Is Distinct from Its Role in Actin Polarity

Joan E. Adamo,*†Guendalina Rossi,* and Patrick Brennwald*†‡

*Department of Cell Biology and †Graduate Program in Molecular Biology, Cell Biology, and Genetics, Weill Medical College of Cornell University, New York, New York 10021

Submitted June 16, 1999; Accepted October 7, 1999
Monitoring Editor: Juan Bonifacino

Budding yeast grow asymmetrically by the polarized delivery of proteins and lipids to specific sites on the plasma membrane. This requires the coordinated polarization of the actin cytoskeleton and the secretory apparatus. We identified Rho3 on the basis of its genetic interactions with several late-acting secretory genes. Mutational analysis of the Rho3 effector domain reveals three distinct functions in cell polarity: regulation of actin polarity, transport of exocytic vesicles from the mother cell to the bud, and docking and fusion of vesicles with the plasma membrane. We provide evidence that the vesicle delivery function of Rho3 is mediated by the unconventional myosin Myo2 and that the docking and fusion function is mediated by the exocyst component Exo70. These data suggest that Rho3 acts as a key regulator of cell polarity and exocytosis, coordinating several distinct events for delivery of proteins to specific sites on the cell surface.

INTRODUCTION

Delivery of newly synthesized proteins and lipids to specific sites on the cell surface is critical for the polarized growth observed in many eukaryotic cells. Budding yeast show a high degree of polarity and polarized growth during several stages of their cell cycle (Welch *et al.*, 1994; Lew and Reed, 1995). They are polarized to the presumptive bud site in unbudded cells. Polarized growth occurs at the bud tip in small budded cells, then expands in larger buds, and finally is directed to the mother–daughter neck in cells about to undergo cytokinesis (Lew and Reed, 1995). Protein secretion is also highly polarized and corresponds to the pattern of bud growth (Tkacz and Lampen, 1973; Field and Schekman, 1980). This polarization of a yeast cell involves distinct rearrangements of the actin cytoskeleton and the transport of vesicles to the site of polarized growth (Novick and Botstein, 1985).

Genetic analysis in yeast has identified a number of gene products required for the terminal stages of exocytic trafficking to the cell surface in yeast. These include the unconventional type V myosin Myo2 (Johnston *et al.*, 1991), the rab GTPase Sec4 (Salminen and Novick, 1987), a number of gene products that form a multisubunit complex known as the exocyst (TerBush *et al.*, 1996; Finger *et al.*, 1998; Guo *et al.*, 1999), and the SNAP receptor (SNARE) proteins Snc1/2, Sso1/2, and Sec9 (Aalto *et al.*, 1993; Protopopov *et al.*, 1993; Brennwald *et al.*, 1994). Myo2 is thought to be involved in the polarized delivery of vesicles from the mother cell to the bud (Govindan *et al.*, 1995; Pruyne *et al.*, 1998), whereas the rab, exocyst, and SNARE components all appear to function at the docking and fusion step (Novick and Brennwald, 1993).

The *rho* family of GTPases is thought to have a central role in the polarized growth process (Ridley, 1995; Drubin and Nelson, 1996). Yeast cells contain five *rho* family members: *RHO1*, *RHO2*, *RHO3*, *RHO4*, and *CDC42*. These genes, similar to their mammalian counterparts, play a variety of roles in cell polarity and polarized cell growth (Johnson, 1999; Kroschewski *et al.*, 1999). *RHO1* is essential and is thought to be involved in regulating the synthesis and integrity of the cell wall (Drgonova *et al.*, 1996). *RHO2* is not essential and has overlapping functions with *RHO1* (Madaule *et al.*, 1987). *RHO3* and *RHO4* may have some partially overlapping functions (Matsui and Toh-e, 1992a,b; Kagami *et al.*, 1997) and are thought to play a role in bud formation (Imai *et al.*, 1996). *CDC42* and its guanine nucleotide exchange factor *CDC24* are thought to be the most upstream components in the pathway for polarized bud formation (Pringle *et al.*, 1995; Richman *et al.*, 1999).

A previous report (Imai *et al.*, 1996) suggested a possible connection between Rho3 and the exocytic apparatus by identifying *SEC4* as a multicopy suppressor of a *rho3*Δ strain. However in the analysis of a temperature-sensitive allele of *RHO3* reported in this same study, they were unable to detect any significant defect in the secretion of the exocytic marker invertase (Imai *et al.*, 1996). Here we show a large number of additional genetic interactions between Rho3 and components of the exocytic apparatus, and we demonstrate that Rho3 has a direct role in exocytosis that is independent of its role in regulating actin polarity. Further-

‡ Corresponding author. E-mail address: pjbrennw@mail.med.cornell.edu.

more, analysis of a conditional mutant indicates that the role of Rho3 in exocytosis likely has two components: 1) a myosin (Myo2)-mediated function in the transport of post-Golgi vesicles from the mother cell to the bud and 2) an exocyst (Exo70)-mediated function in the docking and fusion of vesicles with the plasma membrane.

MATERIALS AND METHODS

Yeast Strains, Reagents, and Genetic Techniques

Cells were grown in YPD media containing 1% bacto-yeast extract, 2% bacto-peptone, and 2% glucose, all from Difco (Sparks, MD). For all assays performed, 25°C was the permissive temperature, whereas 14°C was used as the restrictive temperature. Room temperature (RT) was ~22°C.

Sorbitol, sodium azide (NaN_3), *N*-ethylmaleimide (NEM), β-mercaptoethanol, *o*-dianasidine, glucose oxidase, peroxidase, Calcofluor, tetramethylrhodamine isothiocyanate (TRITC)-conjugated phalloidin, Triton X-100, and 3-amino-1,2,4-triazole were obtained from Sigma Chemical (St. Louis, MO). Zymolyase (100T) was from Seikagaku (Tokyo, Japan). BSA and yeast nitrogen base were from US Biologicals (Swampscott, MA). Formaldehyde (37%), gluteraldehyde, and Spurr's resin were from Electron Microscopy Sciences (Ft. Washington, PA).

Transformations for suppression analysis were performed using the lithium acetate method described by Ito *et al.* (1983). Strain crossing, tetrad dissection, diploid sporulation, and mating-type determination were performed as described by Guthrie and Fink (1991).

Generation of Mutations in RHO3

Oligo-directed mutagenesis was performed to create the GTP- and GDP-bound forms of *RHO3*, as well as the pool of effector domain mutations (Kunkel *et al.*, 1987). Fourteen synthetic oligonucleotides were used to change each of the 14 amino acids in the effector domain to other random amino acids. Each oligonucleotide had a mixture of bases at the position where different amino acids were desired and was designed to contain at least 10 bp of homology on both sides of the mixed residue. Resulting mutants were then sequenced to determine the amino acid sequence.

To determine the phenotype of each of the *rho3* mutants as the only source of Rho3, we transformed the constructs into a diploid yeast strain heterozygous for a chromosomal deletion of *RHO3*. BY506 (*a/α; GAL+/GAL+; ura3-52/ura3-52; leu2-3112/leu2-3112; his3-Δ200/his3-Δ200; rho3Δ::LEU2/RHO3*) has one copy of *RHO3* disrupted by the insertion of the *LEU2* marker. The plasmids containing the *rho3* mutant were cleaved within the *URA3* gene to target chromosomal integration at the *URA3* locus. The transformants were colony purified and sporulated, and tetrads were dissected with a micromanipulator on YPD plates. The plates were grown at 25°C. The haploid progeny were then analyzed by replica plating for the presence of the integrated mutants (scored as ura+), for the presence of a disrupted copy of *rho3* (scored as leu+), and for conditional growth at 37 or 14°C.

Invertase Assays

Cells were grown in YPD to midlog phase, diluted back, and preshifted to the restrictive temperature for 1 h (or kept at the permissive temperature). From these cultures, two aliquots of 0.8 OD_{599} U were pelleted. One-half was resuspended in 10 mM NaN_3 and kept on ice, while the other one-half was resuspended in low-glucose (0.1%) YPD and shifted to 14°C for 5 or 10 h or to 25°C for 1.5 h. After the shift, the fractions were resuspended in NaN_3, and aliquots from both fractions were spheroplasted for 30 min at 37°C in a 1.4 M sorbitol and Tris-buffered solution containing β-mercaptoethanol and 0.1 mg/ml 100T zymolyase. Spheroplasted internal fractions were then resuspended in 0.5% Triton X-100.

All internal and external samples were assayed at 37°C in a sodium acetate and NEM buffer by adding 25 μl of 0.5 M sucrose and then stopping the reaction after 15 min with 150 μl of 0.2 M K_2HPO_4. The addition of an assay mix containing NEM, *o*-dianasidine, glucose oxidase, and peroxidase in a 0.1 M KPO_4 buffer causes a color change in the presence of glucose. This end-point assay was fully stopped and developed by the addition of 6 N HCl. Spectrophotometric readings were taken at A_{540}, and units of activity were calculated and reported as micromoles of glucose released per minute per OD_{599} of cells.

Invertase, Bgl2, and Carboxypeptidase Y (CPY) blots

RHO3, *rho3-V51*, and *sec4-P48* cells were grown overnight to midlog phase at 25°C in YPD. Strains were preshifted to the restrictive temperature of 14°C for 1 h before being transferred to YP media containing low (0.1%) glucose for 5 h. In addition, the late-secretory temperature-sensitive mutant *sec18-1* was preshifted to 37°C for 1 h before a 3-h shift into low glucose. Whole-cell glass bead lysates were prepared and boiled with 2× sample buffer. Samples were subjected to SDS-PAGE, transferred to nitrocellulose, and probed with affinity-purified α-invertase antibody at 1:200 or affinity-purified α-CPY antibody at 1:1000. For Bgl2 blots, cells were spheroplasted, and the internal and external fractions were separated. Internal fractions were boiled in 2× sample buffer, and the external fractions were boiled in 6× sample buffer. Samples were subjected to SDS-PAGE, transferred to nitrocellulose, and probed with affinity-purified α-Bgl2 antibody at 1:100.

Wide-Field Fluorescence and Imaging

For actin staining, cells were grown overnight in YPD media to ~0.5 OD_{599}. They were then either shifted to the restrictive temperature of 14°C for 5 h or kept at the permissive temperature before fixative (formaldehyde to 3.7%) was added directly to the media. A second round of fixation was performed in KPO_4 buffer (pH 6.5), and the cells were transferred to a sorbitol buffer for overnight storage at 4°C.

The next day cells were permeabilized for 10 min in 0.1% Triton X-100 and washed twice with PBS. Cells were resuspended in 100 μl of PBS and stained in the dark for 25 min with 35 μl of 3.3 μM TRITC-phalloidin dissolved in methanol. Cells were washed six times with PBS and then resuspended in the appropriate volume of mounting media (90% glycerol with 4′,6-diamidino-2-phenylindol to visualize DNA and *o*-phenylenediamine to retard photobleaching). To study the deposition of chitin in the bud scars, cells from the same round of fixation were not permeabilized, and 3 μl of 1 mg/ml Calcofluor was added instead of labeled phalloidin. Stained cells was viewed on a Nikon Eclipse E600 microscope (Garden City, NY); images were captured with a Princeton Instruments charge-coupled device camera (Trenton, NJ) and Metamorph Imaging software (Universal Imaging, West Chester, PA).

Thin-Section Electron Microscopy

Cells were grown overnight in YPD media to midlog phase and diluted back the next day, and then one-half of the culture was shifted to the restrictive temperature 14°C and grown for 5 h to an OD_{599} of 0.8. Ten optical density units were harvested on a 115-ml, 0.45-μm Nalgene (Rochester, NY) filter, washed with 0.1 M cacodylate, and resuspended in a 0.1 M cacodylate and 3% gluteraldehyde fixative solution. Cells were then allowed to fix for 1 h at RT and then overnight at 4°C. Cells were spheroplasted for 40 min at 37°C in a KPO_4-buffered solution of 0.3 mg/ml zymolyase and then washed with cold cacodylate. Then 1.5 OD U was pelleted in a 1.7-ml microfuge tube and incubated on ice for 1 h at RT with a solution of 2% osmium tetroxide and 0.1 M cacodylate. Pellets were washed three times each with dH_2O and incubated in a 2%

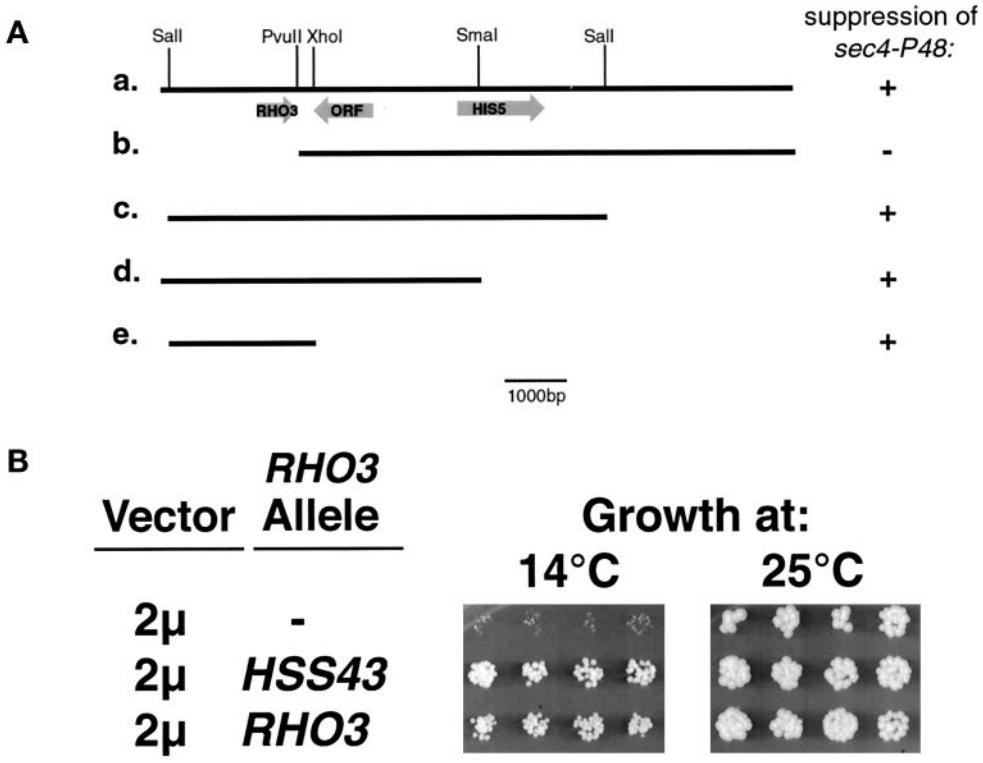

Figure 1. *HSS43* is allelic to *RHO3*. (A) A restriction map of the 10-kb *HSS43*-suppressing fragment and the subclones derived from it are shown. (a) *HSS43* (10 kb). (b) *Pvu*II fragment. (c) *Sal*I fragment. (d) *Sal*I-*Sma*I fragment. (e) *Sal*I-*Xho*I 2.2-kb fragment. (B) The *Sal*I-*Xho*I fragment containing the entire *RHO3* open reading frame (ORF) is exclusively responsible for the suppression seen by *HSS43*.

aqueous solution of uranyl acetate for 1 h at RT in the dark. Each pellet was rinsed twice with dH_2O and taken through the following 10-min ethanol dehydration steps: 50, 70, 85, and 95% and then four rinses in 100% ethanol. The pellet was rinsed once with 100% acetone and then covered with a 50% acetone and 50% Spurr's resin mixture. This remained at RT for 5 h, the acetone and Spurr's resin mixture was replaced with 100% Spurr's resin, and these remained at RT overnight. The 100% Spurr's resin was changed the next day, and the pellets were baked in Spurr's resin for 24 h at 80°C. Thin sections were cut and layered onto an uncoated copper grid and poststained with lead citrate and uranyl acetate before viewing. Cells were viewed on a JEOL 100CXII Electron microscope (Tokyo, Japan) and photographed at 60 kV.

Two-Hybrid Analysis

The constructs were prepared by a recombinational cloning method (Hudson *et al.*, 1997) in which the indicated Rho3 fragments were PCR amplified with 70 bp extensions on each end. These extensions then directed the in vivo incorporation of the fragment into a *Nco*I/*Pvu*II-digested pOBD.CYH vector. Rho3 and activated Rho3-V25 were amplified by PCR, whereas the Rho3-V25,V51 double mutant was generated by fusion PCR, and all were confirmed by DNA sequence analysis. The C-terminal CAAX box was deleted by placing a termination codon in place of the cysteine residue. The *GAL4AD* constructs were made in a similar way and inserted into the activating domain vector pOAD by recombinational cloning. All constructs were tested to verify that they did not interact when paired with the opposing empty vector. Transformants were shown to express the expected size of the *GAL4BD-RHO3* fusion by Western blotting and then transformed with the *GAL4AD-MYO2* or *GAL4AD-EXO70* constructs. Constructs were transformed into the strain PJ694α that has the *HIS3* gene as a reporter (James *et al.*, 1996). To reconfirm that similar amounts of Rho3 fusion proteins were present, immunoblotting of the two-hybrid transformants was performed on whole-cell lysates as described above. Blots were probed with affinity-purified Rho3 antibodies and detected with ^{125}I-protein A.

RESULTS

Identification of RHO3 *as a Suppressor of the* sec4-P48 *Mutant*

We identified previously a number of genes, including the plasma membrane SNARE *SEC9*, on the basis of their ability to act as suppressors of the cold-sensitive Rab GTPase mutant *sec4-P48* (Brennwald *et al.*, 1994). Although *SEC9* was the most potent multicopy suppressor, we describe here the analysis of a second suppressor, *HSS43*, whose strength of suppression was nearly as strong as that of *SEC9*. Analysis of subclones of *HSS43* (Figure 1A) identified the 2.2-kb *Sal*I-*Xho*I fragment that contained the entire open reading frame of *RHO3* as necessary and sufficient to achieve the suppression attributed to *HSS43* (Figure 1B). To determine the specificity of Rho3 in this pathway, we looked at the suppression capabilities of all five of the yeast *RHO* family members. The results shown in Figure 2A demonstrate clearly that this property is highly specific to Rho3 because none of the other *RHO* genes, *RHO1*, *RHO2*, *RHO4*, or *CDC42*, were able to interact genetically with Sec4 in the same way that Rho3 did.

Rho3 is a member of the Ras superfamily of small GTPases that function as molecular switches (Bourne *et al.*, 1991). By analogy to the *ras* oncogene, mutations were made in Rho3 that predict a constitutively active (GTP-bound) or a constitutively inactive (GDP-bound) form. We made two mutations, *RHO3-V25*, equivalent to the activating *ras-V12* mu-

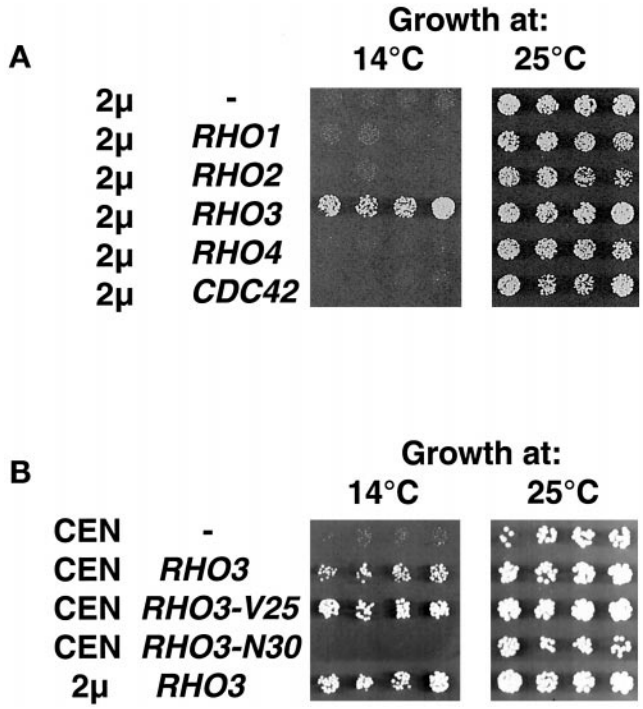

Figure 2. *RHO3* is a specific suppressor of *sec4-P48,* and the GTP-bound form is the active form. (A) *RHO3* is the only one of the five *RHO* genes, *RHO1*, *RHO2*, *RHO3*, *RHO4*, or *CDC42*, that can suppress the cold sensitivity of *sec4-P48*. (B) Activated alleles of *RHO3* suppress at a single copy. *RHO3-V25* has amino acid 25 changed from a glycine to a valine that is analogous to the *ras-V12*-activating mutation. *RHO3-N30* has the threonine at amino acid 30 changed to an asparagine, analogous to the *ras-N17* dominant-inhibitory mutation. Each of these was introduced into *sec4-P48* at a single copy, and transformants were tested for suppression of the cold sensitivity.

tant, and *RHO3-N30*, analogous to the dominant-inhibitory *ras-N17* mutant. We would predict that if the GTP-bound form is the active form in this pathway, there would be suppression at much lower doses of *RHO3-V25* compared with wild type and that the GDP-bound form would fail to suppress. We therefore examined the effect of each of these on single copy (CEN) plasmids and tested their ability to suppress the *sec4-P48* mutant (Figure 2B). Interestingly, a single extra copy of wild-type *RHO3* results in only partial suppression of the cold sensitivity. However activated *RHO3-V25* on a single copy shows suppression equivalent to that observed with wild-type *RHO3* on high copy. In contrast, the *RHO3-N30* allele, predicted to be in the GDP-bound form, not only fails to suppress but is growth inhibitory.

RHO3 *Shows Multiple Genetic Interactions with Components of the Exocytic Apparatus*

In addition to testing the ability of *RHO3* to suppress *sec4-P48*, we examined the ability of the original clone *HSS43* and the *RHO3* subclone to suppress all of the 10 late-acting *sec* genes. We found that *HSS43* and *RHO3* show a significant level of suppression of both *sec15-1* and *sec8-9* (Brennwald *et al*., 1994) (our unpublished results). Both of these genes are components of the exocyst, a peripherally associated plasma membrane complex thought to aid docking and fusion of vesicles (TerBush and Novick, 1995).

In addition, a number of late-acting secretory genes have been found to suppress *rho3* mutants. Both *SEC9* and *SEC4* act as high-copy suppressors of *rho3* (Imai *et al*., 1996; Lehman *et al*., 1999). *SRO7* and *SRO77* were first identified as high-copy suppressors of a *rho3* mutant (Kagami *et al*., 1998). We have shown recently that Sro7 and Sro77 are Sec9-binding proteins and that loss of these gene products results in a block in Golgi-to-cell-surface transport (Lehman *et al*., 1999).

To look for additional connections between *rho3* and the exocytic apparatus, we used a galactose turn-off assay to identify genes that could rescue the extremely slow growth phenotype of *rho3*Δ cells. Cells with the sole copy of *RHO3* under the control of a Gal promoter were transformed with a genomic library prepared in a 2μ vector. Transformants were selected on glucose-containing media to repress expression of Rho3. Plasmids were isolated from colonies showing growth on glucose, retested for suppression, and sequenced. This resulted in the identification of four distinct suppressing loci (in addition to *RHO3*). Two of these contained genes shown previously to suppress *rho3* mutants, *SEC4* and *BEM1*, a gene shown to be involved in bud formation and cell polarity. Three independent clones contained overlapping segments of the t-SNARE *SSO2*; subcloning revealed this gene to be necessary and sufficient for the suppressing activity. The fourth gene is still being characterized and will be described elsewhere. In summary, four distinct components of the exocytic machinery, Sec4, Sec9, Sro7, and Sso2, can act as suppressors of *rho3*Δ mutants. This demonstrates that loss of Rho3 function is most readily assisted by increasing the function of the exocytic machinery. These numerous genetic interactions strongly suggest that Rho3 plays a critical role in exocytosis.

Mutational Analysis of the RHO3 *Effector Domain*

We hypothesized that the above genetic evidence suggests an additional critical role for Rho3 in exocytosis, independent of its role in actin polarity maintenance. This is consistent with the rapidly growing body of evidence that Rho GTPases often have a large number of effectors that can cover a diverse range of functions (Tapon and Hall, 1997; Aspenström, 1999). In an attempt to reveal a direct role of Rho3 in exocytosis and to distinguish this role from the role of *RHO3* in actin polarity, we initiated an extensive mutagenesis of the effector domain. This highly conserved region has been shown to be critical for interactions between *ras* GTPase superfamily members and their downstream effectors (Bourne *et al*., 1991).

The region of Rho3 known as the effector domain can be aligned with the same conserved domains from other proteins such as H-ras and Cdc42 (Figure 3A). The results of the oligo-directed mutagenesis are listed in Figure 3B. Mutant alleles were introduced into yeast and tested for their ability to function as the only copy of *RHO3*. Of the 46 mutants examined, all were recessive, and 30 were indistinguishable from wild type under the conditions tested. Eleven mutants failed to rescue the severe growth

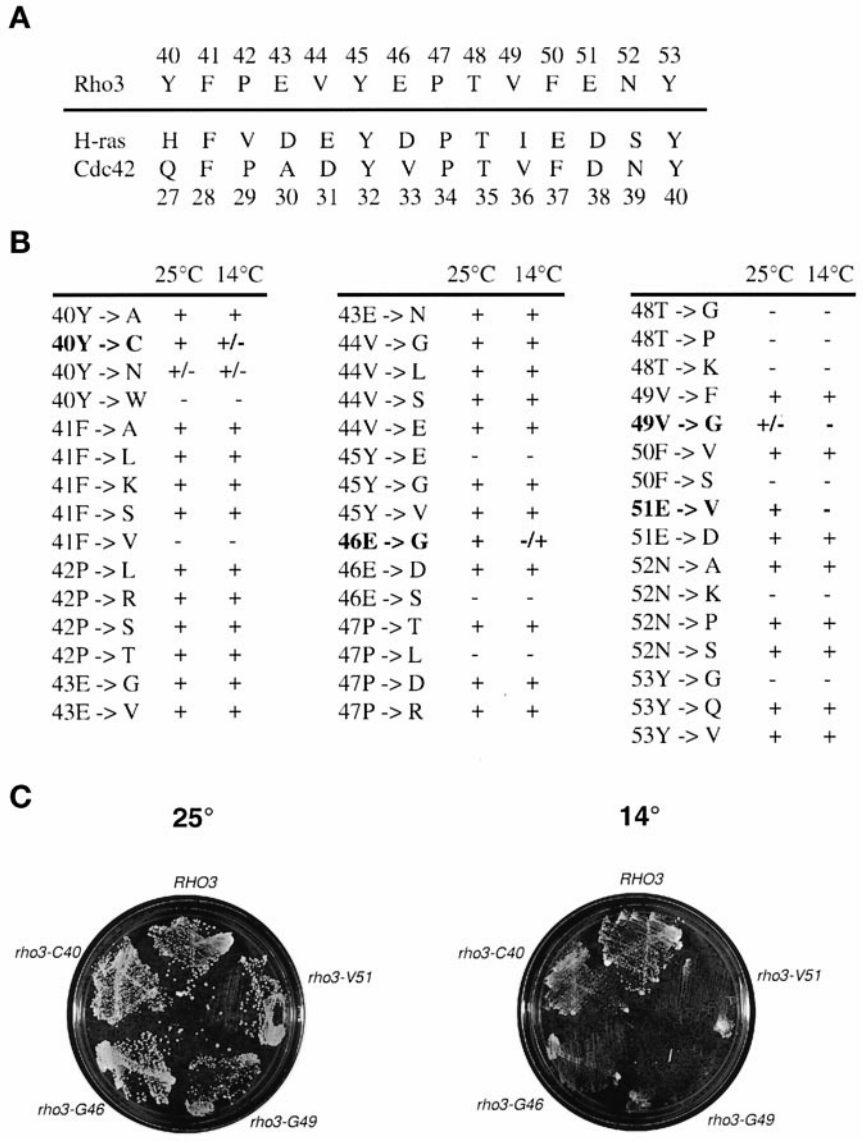

A

	40	41	42	43	44	45	46	47	48	49	50	51	52	53
Rho3	Y	F	P	E	V	Y	E	P	T	V	F	E	N	Y
H-ras	H	F	V	D	E	Y	D	P	T	I	E	D	S	Y
Cdc42	Q	F	P	A	D	Y	V	P	T	V	F	D	N	Y
	27	28	29	30	31	32	33	34	35	36	37	38	39	40

B

	25°C	14°C
40Y -> A	+	+
40Y -> C	+	+/-
40Y -> N	+/-	+/-
40Y -> W	-	-
41F -> A	+	+
41F -> L	+	+
41F -> K	+	+
41F -> S	+	+
41F -> V	-	-
42P -> L	+	+
42P -> R	+	+
42P -> S	+	+
42P -> T	+	+
43E -> G	+	+
43E -> V	+	+

	25°C	14°C
43E -> N	+	+
44V -> G	+	+
44V -> L	+	+
44V -> S	+	+
44V -> E	+	+
45Y -> E	-	-
45Y -> G	+	+
45Y -> V	+	+
46E -> G	+	-/+
46E -> D	+	+
46E -> S	-	-
47P -> T	+	+
47P -> L	-	-
47P -> D	+	+
47P -> R	+	+

	25°C	14°C
48T -> G	-	-
48T -> P	-	-
48T -> K	-	-
49V -> F	+	+
49V -> G	+/-	-
50F -> V	+	+
50F -> S	-	-
51E -> V	+	-
51E -> D	+	+
52N -> A	+	+
52N -> K	-	-
52N -> P	+	+
52N -> S	+	+
53Y -> G	-	-
53Y -> Q	+	+
53Y -> V	+	+

C

Figure 3. Mutagenesis of the Rho3 effector domain. (A) Alignment of the 14 amino acids of the effector domains of Rho3, H-ras, and Cdc42. (B) Forty-six single-point mutations generated by oligo-directed mutagenesis. Growth at each temperature was recorded as follows: (+) = wild-type growth, (+/−) = borderline growth, (−/+) = slight growth above background, and (−) = no growth. (C) Growth of the *rho3* mutants at the permissive and restrictive temperature. Plates at 25°C were incubated for 4 d, and plates at 14°C plates were incubated for 7 d.

defect associated with the *rho3*Δ deletion, and 1 mutant rescued slightly but gave constitutively slow growth under all conditions tested. Four mutants showed relatively normal growth at 25°C but showed significantly reduced growth at 14°C (Figure 3, these last four are shown in bold type). Figure 3C shows the growth of four cold-sensitive mutants at 14°C as compared with wild type and compared with their growth at the permissive temperature of 25°C. None of the mutants showed sensitivity to growth at high temperature (37°C) in this study. Bright-field analysis of all four of the mutants revealed an increase in cell size, a phenotype often associated with defects in cell polarity (Novick and Botstein, 1985). But this enlargement was not dependent on the temperature shift in any of the cells, and the most dramatic size increase was seen in the mutant *rho3-C40* (our unpublished results).

Analysis of the Actin Cytoskeleton in rho3 *Mutants*

Loss of Rho3 function has been shown previously to cause an altered distribution in the normally highly polarized actin cytoskeleton (Imai *et al.*, 1996). We therefore examined the status of the actin cytoskeleton in the four cold-sensitive *rho3* mutants by rhodamine phalloidin staining. Both actin filaments and cortical actin patches show a very high degree of polarity in yeast (Welch *et al.*, 1994; Lew and Reed, 1995; Karpova *et al.*, 1998). In wild-type cells, cortical actin is highly polarized and found almost exclusively in the bud (Welch *et al.*, 1994; Lew and Reed, 1995). Only as the cell nears cytokinesis do the cortical patches become significantly apparent in the mother cell. Actin cables are normally oriented along the mother–bud axis.

Cells were examined after growth at 25°C or after a 5-h shift to 14°C. As expected, several of the effector mutants demon-

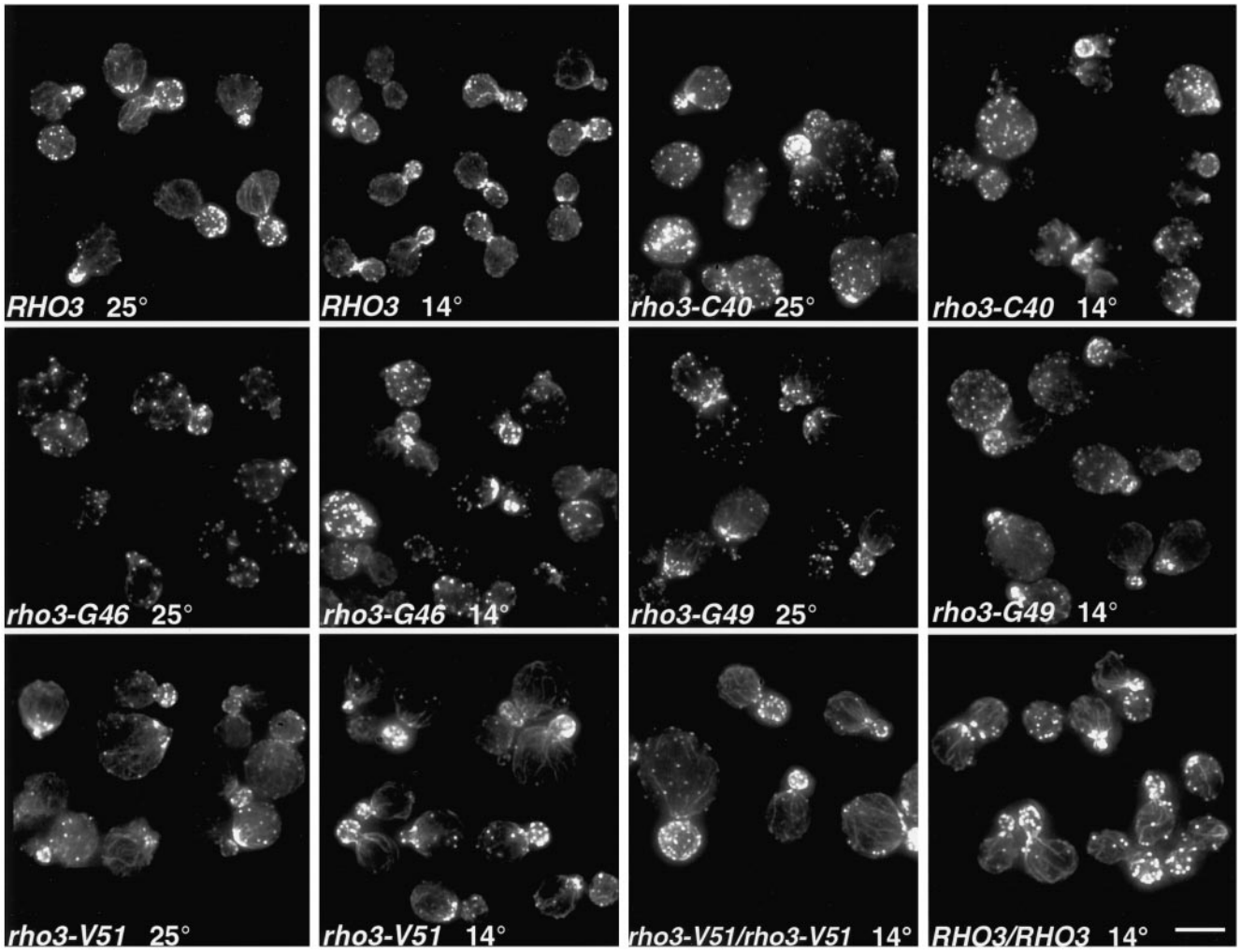

Figure 4. Actin localization in wild-type and *rho3* mutant cells. Cells were grown at 25°C or shifted to 14°C for 5 h before fixation. Fixed cells were subsequently permeabilized and stained as described in MATERIALS AND METHODS. Bar, 5 μm.

strated pronounced defects in actin polarity (Figure 4). Three of the mutants show a loss of the normal actin patterns. In particular the most severe defects were seen in *rho3-C40* and *rho3-G46*. They showed almost complete loss of cables and random distribution of cortical patches. *rho3-G49* showed a partial loss of cables and a disruption of cortical patch polarization. In all three of these mutants, the actin polarity defects appeared to be similar at both temperatures.

In contrast, the *rho3-V51* mutant had a normal and polarized actin cytoskeleton that was indistinguishable from the polarized actin in wild-type cells at both 25 and 14°C. As with wild-type cells, the cortical actin patches were well polarized to the bud. The cables were clearly present, well organized, and of normal length relative to cell size (i.e., because *rho3-V51* cells are larger, the cables are proportionally longer). We also examined diploids homozygous for the *rho3-V51* mutation and found they also showed staining patterns identical to that of wild-type diploids at both the permissive (our unpublished results) and restrictive temperatures (Figure 4).

The proper formation of chitin scars at bud sites is dependent on the polarization of actin (Chant and Pringle, 1991). We therefore looked for bud site selection defects in a subset of these *rho3*Δ mutants by staining chitin with the fluorescent dye Calcofluor. The results demonstrate that *rho3-V51* exhibited normal budding patterns in both haploids and homozygous diploids, and in contrast, the *rho3-C40* mutant and, to a somewhat lesser extent, the other mutants showed aberrant bud site selection and delocalized chitin deposition (our unpublished results). This provides additional evidence that out of the four cold-sensitive effector mutants, only *rho3-V51* is fully functional in regulation of the actin cytoskeleton.

The rho3-V51 *Mutant Has a Post-Golgi Secretory Defect*

To determine whether the actin-independent growth defect associated with the *rho3-V51* mutant was caused by a defect in the exocytic function of these cells as predicted by the

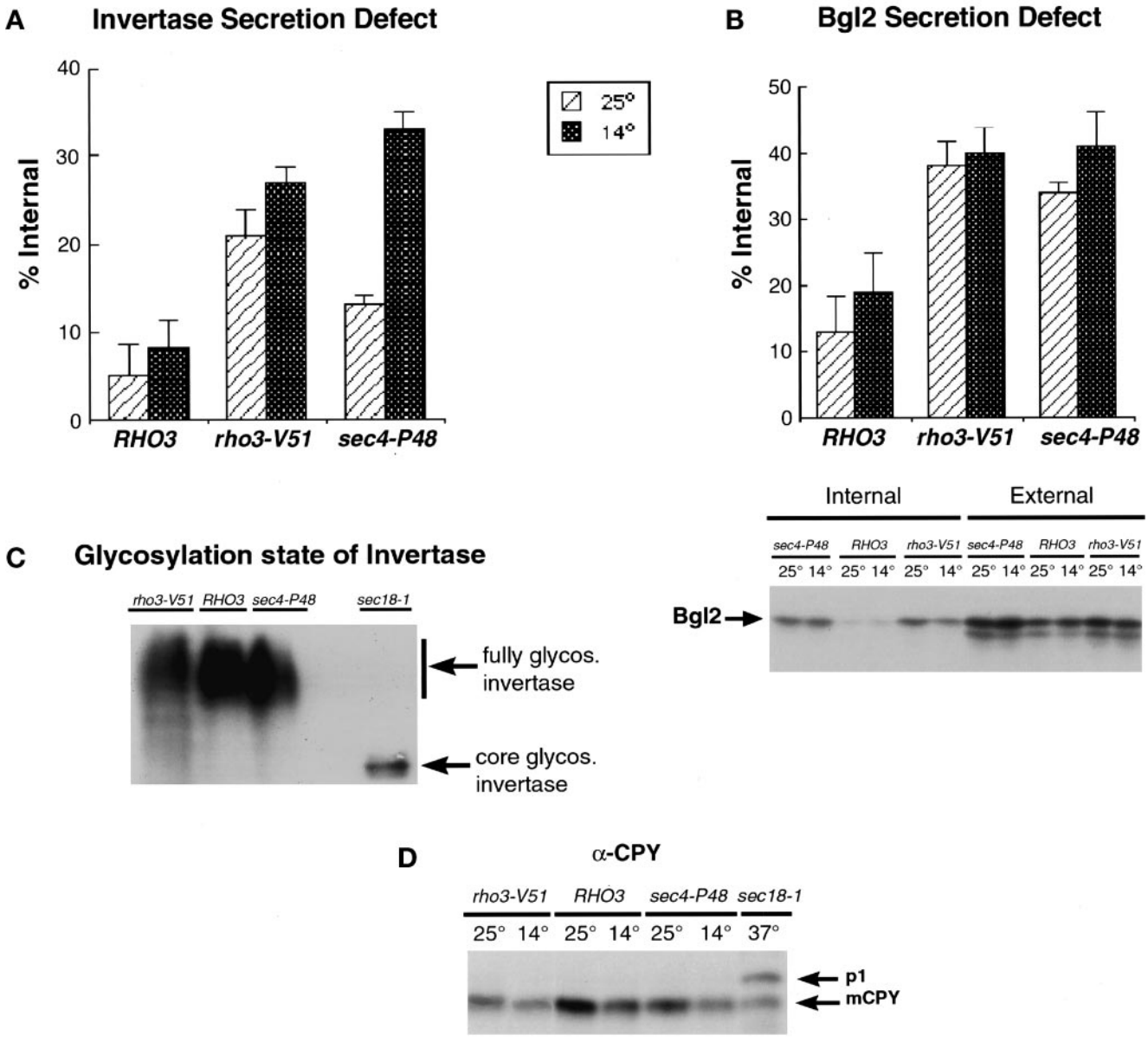

Figure 5. The *rho3-V51* mutant is defective in the secretion of the periplasmic enzymes invertase and Bgl2. (A) Invertase enzyme assays show a defect in the secretion for *rho3-V51* at both the permissive and restrictive temperature. Secretion assays are presented as a percentage of invertase that is found internally. This is a positive measure of the secretory defect associated with a particular strain. This percentage of internal invertase is calculated by internal/(internal + external), where these values are measured as micromoles per minute per OD_{599}. The data represent the average ± SD for five assays. (B) Immunoblot analysis of Bgl2 protein distribution shows a defect in secretion for *rho3-V51* at both the permissive and restrictive temperature. The distribution of the secreted protein Bgl2 was determined by immunoblot analysis using affinity-purified antibodies raised against the C terminus of Bgl2. The band corresponding to Bgl2 is indicated. Top, quantitation of the bands was done using ImageQuant software (Molecular Dynamics, Sunnyvale, CA). The results are presented as a percentage of the total Bgl2 that is found internally. The data represent the average ± SD for three experiments. Bottom, a representative Bgl2 blot is shown. (C) Immunoblot analysis of invertase reveals the glycosylation state of invertase in these cells. (D) Transport of the vacuolar protein CPY is not affected in *rho3-V51*, because it is found exclusively in the mature form (mCPY, 61 kDa) at both temperatures. A *sec18-1* mutant was included as a size marker and exhibits accumulation of the core glycosylated form (p1, 67 kDa). glycos., glycosylated.

abundance of genetic data described above, we examined the ability of these strains to export two periplasmic proteins, invertase and Bgl2. Both of these proteins are dependent on the classical secretory pathway for their delivery to the cell surface (Kaiser *et al.*, 1996). *RHO3*, *rho3-V51,* and *sec4-P48* strains were shifted to low glucose to derepress the

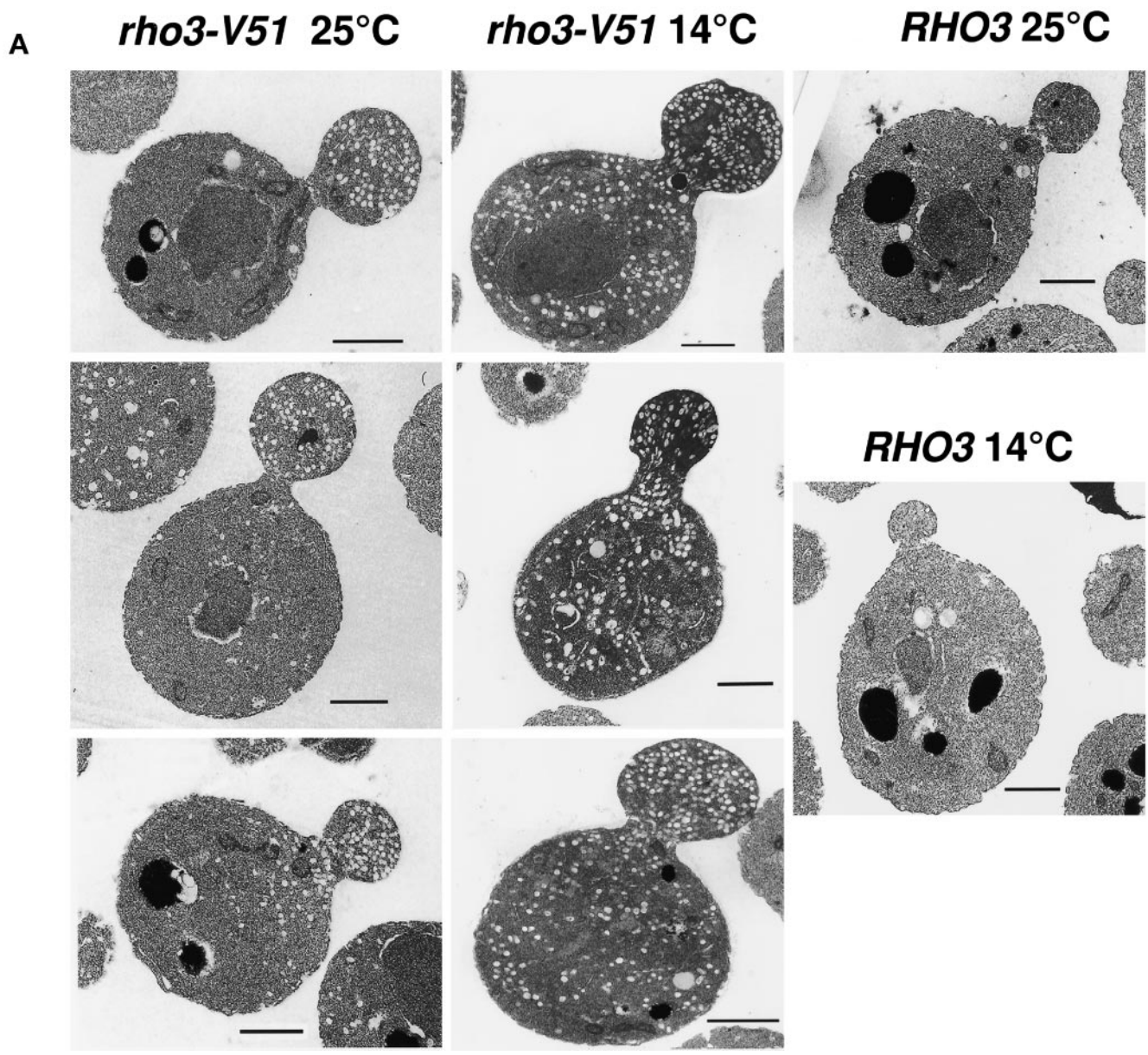

Figure 6. Electron microscopy of *rho3-V51* cells reveals accumulation of post-Golgi vesicles and a conditional defect in vesicle delivery from the mother to the bud. (A) Three panels of *rho3-V51* at both 25 and 14°C as well as single panels of *RHO3* at 25 and 14°C are shown. Preparation of the cells is described in MATERIALS AND METHODS. (B) Cells were scored for the location of accumulated vesicles, and bar graphs show the percentage of cells with vesicles in the bud/neck region, in the mother cell, and in the entire cell. Approximately 30 cells were counted for *rho3-V51* at each temperature, and 20 cells were counted for the *RHO3* cells (wt). Only small budded cells were counted. Bars, 1 μm.

production of invertase at either 25 or 14°C. The amount of internal and external enzyme activity was determined in five separate experiments, and the amount of invertase in the internal fraction is shown in Figure 5A. As expected, the *sec4-P48* mutant shows a defect at 14°C but secretes well at 25°C. In agreement with the prediction that Rho3 has a direct role in exocytosis, the *rho3-V51* cells display a pronounced defect in invertase secretion similar to that of *sec4-P48*. Although wild-type cells were able to secrete 92% of invertase and retained only 8% in the internal fraction at 14°C, the *sec4-P48* mutant retained 33%, and *rho3-V51* retained 27% in the internal fraction at the restrictive temperature. Surprisingly, when tested at 25°C, the *rho3-V51* mutant showed a significant defect in exocytosis at the permissive temperature (21% internal invertase for *rho3-V51* compared with only 5% for wild-type cells).

We also examined the ability of the other mutants to secrete invertase after a 5-h shift to 14°C. They were found to

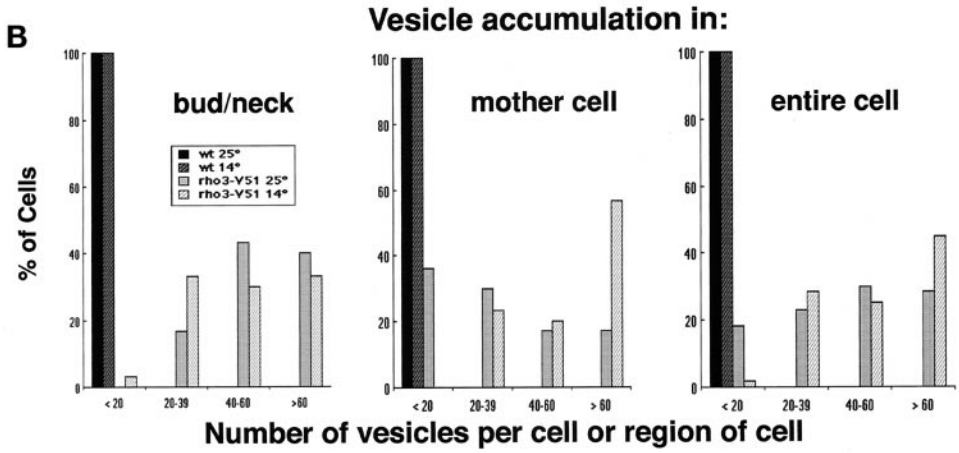

Figure 6 (cont.)

be significantly less defective in secretion: 17 ± 9.8% (*rho3-C40*), 10 ± 6.5% (*rho3-G46*), and 16 ± 9.6% (*rho3-G49*). However, because defects in actin have been shown previously to cause defects in secretion (Novick and Botstein, 1985), it is unclear whether these partial defects are associated with a direct effect on the secretory capacity versus an indirect effect resulting from a depolarized actin cytoskeleton.

Immunoblot analysis with α-invertase antibodies showed that virtually all of the invertase in the cells migrated as the fully glycosylated form, demonstrating that the defect is likely to be at the post-Golgi stage of secretion (Figure 5C). Consistent with a post-Golgi defect, maturation and transport of CPY appear to be unaffected. Immunoblots of these cells show that only the mature form is present in *rho3-V51* as in wild-type and *sec4-P48* (Figure 5D). In addition, pulse-chase analysis of CPY maturation demonstrated that there was no defect in the kinetics of transport of CPY to the vacuole (our unpublished results).

Two classes of vesicles have been demonstrated to be involved in post-Golgi delivery to the plasma membrane (Harsay and Bretscher, 1995). Invertase is specific to the lighter class of vesicles, and Bgl2, a cell wall endoglucanase, has been shown to be specific to the denser class of vesicles. To determine whether both classes of vesicles were affected, we examined the secretion of Bgl2 in the *rho3-V51* and *sec4-P48* cells. Immunoblots were used to probe the internal and external fractions at both the permissive and restrictive temperatures. Figure 5B shows the results of Bgl2 secretion assays that are expressed as the percentage of Bgl2 found internally. In agreement with the results seen for the secretion of invertase above, *rho3-V51* shows a pronounced defect in the secretion of Bgl2 at both 25 and 14°C. Although wild-type *RHO3* cells show small internal pools of only 13 and 19% at 25 and 14°C, the *rho3-V51* cells show much larger internal pools of 38 and 40%, respectively. The quantitation is the mean ± SD of three assays, and a representative blot is shown (Figure 5B, bottom). The identity of the bottom band seen in all the external fractions is unknown and was not included in the quantitation. This defect in Bgl2 secretion indicates that the *rho3-V51* mutant is affecting both classes of vesicles. Interestingly, the *sec4-P48* mutant appears to be less temperature dependent in its secretion of Bgl2 than invertase because it shows defects at both temperatures.

rho3-V51 *Shows a Cold-Sensitive Defect in the Delivery of Vesicles from Mother to Bud*

To examine the exocytic defect in greater detail, we examined *rho3-V51* mutant cells by electron microscopy. All of the post-Golgi–blocked secretory mutants show an accumulation of 80- to 100-nm vesicles. These vesicles are only rarely seen in wild-type cells because their rate of fusion with the bud tip plasma membrane is very rapid. Because the *rho3-V51* mutants had secretory defects at both ambient and low temperatures, we examined the morphology of cells grown with and without a 5-h shift to 14°C. Consistent with the secretory defect seen at 25°C, the *rho3-V51* mutant shows a large accumulation of 80- to 100-nm vesicles. The vesicles appear to be present primarily in the bud and neck region of the cells (Figure 6A, left). In contrast, although *rho3-V51* cells grown at 14°C had a slight increase in the total number of vesicles per cell, a dramatic shift was observed in the location of the vesicles within the cell. Although mother cells with large numbers of vesicles were rare at 25°C, an abundant accumulation of vesicles in the mother cells was observed after a 5-h shift to 14°C (Figure 6A, middle). Wild-type *RHO3* cells are also shown in Figure 6A, right. The quantitation of the vesicle accumulation phenotype is shown as a bar graph (Figure 6B). At 14°C, there is a dramatic shift in the distribution of vesicles within the cell; 60% of the mother cells contained >60 vesicles, whereas <20% of the cells at the permissive temperature fall into this category. This demonstrates that the *rho3-V51* mutant has a cold-sensitive defect in the transport of vesicles from the mother cell into the bud.

The V51 Mutation in Rho3 Results in a Loss of the Interaction with Myo2 and Exo70

A recent study identified fragments of Exo70- and Myo2-coding sequences in a two-hybrid screen for potential effectors of Rho3 (Robinson *et al.*, 1999). To determine whether the exocytic defects associated with *rho3-V51* might be a result of a defect in interaction with these

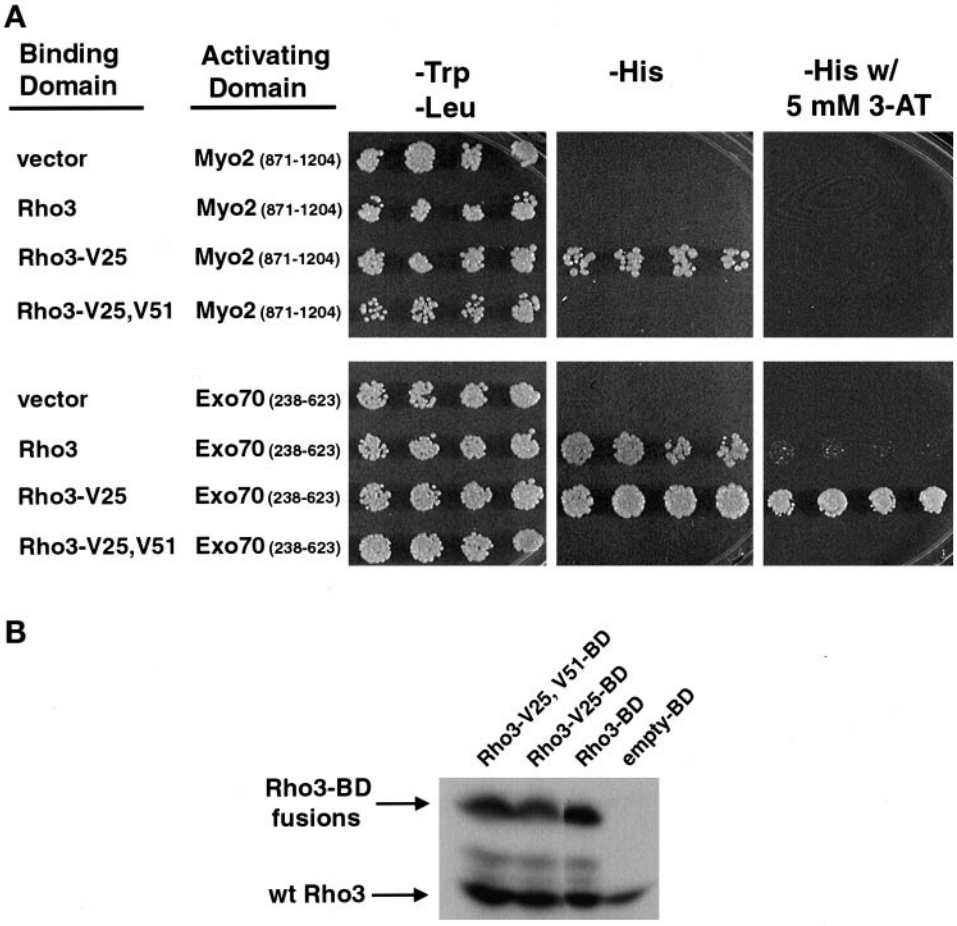

Figure 7. Two-hybrid analysis of the effect of the V51 mutation on the interaction of Rho3 with Myo2 and Exo70. (A) Two-hybrid analysis of Rho3, Rho3-V25, and Rho3-V25,V51 mutants on the interaction with Myo2 and Exo70. Constructs containing *GAL4BD-RHO3* and the *GAL4AD-MYO2* (encoding residues 871-1024) or *EXO70-GAL4AD* (encoding residues 238–623) were transformed into PJ694α. Four independent transformants were replicated onto media selecting for both plasmids (−Trp, −Leu) or media that require activation of the *HIS3* reporter (−His), and interactions were assayed by the ability of the two *GAL4* fusions to activate the reporter gene *HIS3*. Growth on media lacking histidine or on media lacking histidine with 5 mM 3-aminotriazole (3-AT), which functions as an inhibitor of the histidine biosynthetic pathway and requires a higher level of *HIS3* activation to support growth, is shown. (B) Western blot analysis of Rho3 protein levels in the two-hybrid transformants using affinity-purified α-Rho3 antibodies. Cotransformants were examined for the expression of the Gal4-binding domain (BD) fusion proteins. The endogenous Rho3 protein migrates at ~29 kDa, and a larger fusion protein of the expected size is visible migrating at ~48 kDa.

candidate effectors, we examined the effect of the *rho3-V51* mutation on this interaction. We made use of the same regions of *MYO2* and *EXO70* identified by Robinson *et al.* (1999), fused to the activation domain of *GAL4*, whereas the *RHO3* alleles were fused to the DNA-binding domain of *GAL4*. In this assay, we made use of the *HIS3* gene as a reporter of activation by the two-hybrid constructs. Activation of this reporter results in growth in the absence of histidine. The strength of interaction can be monitored in part by the sensitivity of growth to the presence of 3-aminotriazole, an inhibitor of the histidine biosynthetic pathway. As can be seen in Figure 7A, a portion of the *MYO2* neck and tail region (amino acids 871-1204) interacts specifically with the activated allele of *RHO3*, *RHO3-V25*. However, the introduction of the *V51* effector mutation into *RHO3-V25* completely abolishes the interaction with *MYO2*. Like *MYO2*, the C-terminal portion of *EXO70* shows both a strong interaction with the activated *RHO3-V25* as well as a weaker interaction with the wild-type form of *RHO3*. The strength of the interaction between activated *RHO3-V25* and *EXO70* is apparent because growth occurs when 5 mM 3-aminotriazole is present and persisted even in the presence of 40 mM 3-aminotriazole (Figure 7A; our unpublished results). As was the case with the *MYO2* interaction the presence of the *V51* mutation in the activated form of *RHO3* leads to a complete loss of growth even on −His media lacking 3-aminotriazole (Figure 7A). Therefore, the *rho3-V51* mutation leads to a loss of the ability of Rho3 to interact with both Myo2 and Exo70. This is consistent with the vesicle delivery defects we observe at 14°C being attributable to a loss of interaction with Myo2 and with the docking and fusion

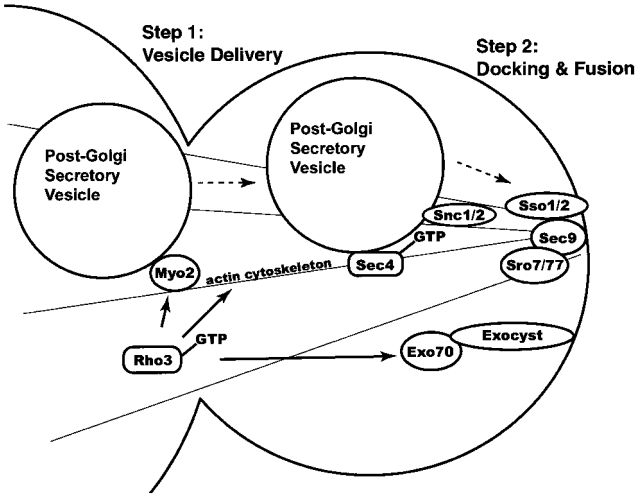

Figure 8. A model for the involvement of Rho3 in two steps of exocytosis. GTP-bound Rho3 appears to have three distinct effector pathways. Previous work (Matsui and Toh-e, 1992b; Imai *et al.*, 1996) and results presented here show a role for Rho3 in regulating the polarized distribution of the actin cytoskeleton. Here we demonstrate a role for Rho3 in exocytosis that is independent of its effect on the actin cytoskeleton. In particular, genetic and electron microscopy data suggest that Rho3 acts both in the delivery of Golgi-derived vesicles from the mother to the bud (Step 1) and in the docking and fusion of these vesicles with the plasma membrane (Step 2). The data presented here provide strong support for the model suggested by the two-hybrid interactions identified by Robinson *et al.* (1999). Therefore our analysis of the *rho3-V51* effector domain mutant supports the model that the vesicle delivery function of Rho3 (Step 1) is mediated by Myo2 and that the vesicle docking and fusion function of Rho3 (Step 2) is mediated by Exo70.

defects observed at 25°C being attributable to defects in interaction with the Exo70 component of the exocyst complex (TerBush *et al.*, 1996).

DISCUSSION

Analysis of an extensive collection of mutants in the effector domain of Rho3 allowed us to separate the exocytic function of Rho3 from its role in regulating actin localization. Our results demonstrate that Rho3 acts as a key regulator of cell polarity by coordinating two important cellular processes: 1) maintenance and localization of the actin cytoskeleton and 2) the polarized delivery, docking, and fusion of post-Golgi secretory vesicles with the plasma membrane. Genetic evidence gave us the first clues concerning a possible role for Rho3 in exocytosis, but it was the mutagenesis of the effector domain in particular that allowed us to discriminate clearly its role in exocytosis from its role in actin polarity. Of the four loss-of-function mutations that we studied, three showed clear actin polarity defects, whereas the fourth showed no defects in actin polarity but had an exocytic defect. It was especially important to distinguish between these two possibilities because actin mutants are known to cause defects in post-Golgi trafficking (Novick and Botstein, 1985).

Our results suggest that Rho3 regulates cell polarity by simultaneously directing the rearrangements of the actin cytoskeleton and the polarized delivery and fusion of the vesicles to specific sites on the cell surface. This is clearly important because these are both dynamic processes in yeast cells. Although the bud tip is the major destination of polarized growth early in the cell cycle, growth becomes isotropic later in the cell cycle. The site of actin polarity and delivery reorients itself to the mother–bud neck, just before cytokinesis. Rho3 could be acting to maintain the proper synchronized actions of actin and vesicle transport; both in specifying a new site and in maintaining delivery to the current site.

In this view, it is especially interesting to find evidence that Rho3 functions in two separate steps of exocytosis: the delivery of vesicles and the docking and fusion of the vesicles. Rho3 shows a number of strong genetic interactions with gene products involved in this second step of the docking and fusion of secretory vesicles at the plasma membrane. In particular, *rho3*Δ was suppressed by the two t-SNAREs Sec9 and Sso2, as well as by the Sec9-binding protein Sro7 (Kagami *et al.*, 1998; Lehman *et al.*, 1999). In addition, there are strong interactions with two subunits of the exocyst complex and the Rab GTPase Sec4. Recent data have suggested that the Rab GTPase and exocyst complex function as tethering factors and work just upstream of SNAREs in driving the vesicles to initiate the fusion reaction (Pfeffer, 1999). Presumably the genetic interactions between these components reflect the role of Rho3 in the docking and fusion step.

With respect to the vesicle delivery step, a conditional defect was apparent when electron microscopy revealed that a shift to 14°C resulted in a very clear accumulation of vesicles in the mother cell. Because vesicles are thought to be primarily produced in the mother cell, they must be delivered to their site of fusion in the bud, so an accumulation of vesicles in the mother cell is a result of a defect in this vectorial delivery process. This cold-sensitive delivery phenotype of Rho3 is strikingly similar to the phenotype of an unconventional type V myosin Myo2 mutant (*myo2-66*) that shows a conditional accumulation of vesicles in the mother cell at the nonpermissive temperature (Govindan *et al.*, 1995).

Recently, Robinson *et al.* (1999) isolated two candidate effectors of Rho3 using a two-hybrid screen. This resulted in the identification of Myo2 and Exo70 as proteins that specifically interact with the GTP-bound form of Rho3. Our analysis of the *rho3-V51* mutant gives strong evidence that Myo2 and Exo70 are likely to be bona fide effectors of Rho3 function in exocytosis. In particular the loss of binding interaction, as measured by two-hybrid analysis, between *rho3-V51* and both *MYO2* and *EXO70* strongly supports the idea that it is a defect in interaction with these two factors that is responsible for the exocytic defects we observe in this mutant. In addition the constitutive exocytic defect of the *rho3* mutants may be caused by a defect in the activation of the exocyst complex via Exo70. The electron microscopy of the mutant under permissive conditions supports this idea. The accumulation of vesicles in the bud and not in the mother in *rho3-V51* cells at 25°C suggests a defect at the docking and fusion stage. This is similar to the phenotype observed in temperature-sensitive mutations in components

of the exocyst complex after a brief shift to 37°C (Govindan *et al*., 1995).

Taken together, these data suggest a model, shown in Figure 8, in which Rho3 acts as a key regulator of polarized trafficking by coordinating three distinct effector pathways. One pathway involves the regulation of the actin cytoskeleton, whereas the other two pathways involve exocytic transport to the cell surface. This includes the regulation of a Myo2-dependent delivery of vesicles from the mother cell to the bud (Figure 8, Step 1) and regulation of an Exo70-dependent docking and fusion of vesicles at specific sites on the plasma membrane (Step 2). These data give us an outline of the function of Rho3 in exocytosis and cell polarity and place it as a key step in the coordinate regulation of these two essential processes. Future work will no doubt unravel the precise mechanisms by which Rho3 effects these functions.

ACKNOWLEDGMENTS

The authors are especially grateful to Dr. Geri Kreitzer and Dr. Enrique Rodriguez-Boulan for allowing us use of their microscope and their expertise and assistance with the fluorescence microscopy and image analysis. We also thank Henry Hamilton for generation of the *RHO3-V25* and *RHO3-N30* mutants, Linda Burg-Freedman and Lee Cohen-Gould for assistance with electron microscopy, Dr. Doug Johnson and Dr. Mike Snyder for plasmids, and Dr. Ruth Collins, Dr. Tim McGraw, Luba Katz, Mayya Maksimova, and Greg St. John for critical reading of the manuscript. This work was supported by grants from the Mathers Charitable Foundation and the Pew Scholars in Biomedical Sciences Program and by the National Institutes of Health grant GM-54712.

REFERENCES

Aalto, M.K., Ronne, H., and Keranen, S. (1993). Yeast syntaxins Sso1p and Sso2p belong to a family of related membrane proteins that function in vesicular transport. EMBO J. *12*, 4095–4104.

Aspenström, P. (1999). Effectors for the Rho GTPases. Curr. Opin. Cell Biol. *11*, 95–102.

Bourne, H.R., Sanders, D.A., and McCormick, F. (1991). The GTPase superfamily: conserved structure and molecular mechanism. Nature *349*, 117–127.

Brennwald, P., Kearns, B., Champion, K., Keranen, S., Bankaitis, V., and Novick, P. (1994). Sec9 is a SNAP-25-like component of a yeast SNARE complex that may be the effector of Sec4 function in exocytosis. Cell *79*, 245–258.

Chant, J., and Pringle, J.R. (1991). Budding and cell polarity in *Saccharomyces cerevisiae*. Curr. Opin. Genet. Dev. *3*, 342–350.

Drgonova, J., Drgon, T., Tanaka, K., Kollar, R., Chen, G.C., Ford, R.A., Chan, C.S., Takai, Y., and Cabib, E. (1996). Rho1p, a yeast protein at the interface between cell polarization and morphogenesis. Science *272*, 277–279.

Drubin, D.G., and Nelson, W.J. (1996). Origins of cell polarity. Cell *84*, 335–344.

Field, C., and Schekman, R. (1980). Localized secretion of acid phosphatase reflects the pattern of cell surface growth in *Saccharomyces cerevisiae*. J. Cell Biol. *86*, 123–128.

Finger, F.P., Hughes, T.E., and Novick, P. (1998). Sec3p is a spatial landmark for polarized secretion in budding yeast. Cell *92*, 559–571.

Govindan, B., Bowser, R., and Novick, P. (1995). The role of Myo2, a yeast class V myosin, in vesicular transport. J. Cell Biol. *128*, 1055–1068.

Guo, W., Roth, D., Walch-Solimena, C., and Novick, P. (1999). The exocyst is an effector for Sec4p, targeting secretory vesicles to sites of exocytosis. EMBO J. *18*, 1071–1080.

Guthrie, C., and Fink, G. (1991). Guide to yeast genetics and molecular biology. In: Methods in Enzymology, vol. 194, ed. J.N. Abelson and M.I. Simon, San Diego: Academic Press, 77–110.

Harsay, E., and Bretscher, A. (1995). Parallel secretory pathways to the cell surface in yeast. J. Cell Biol. *131*, 297–310.

Hudson, J., *et al*. (1997). The complete set of predicted genes from the *Saccharomyces cerevisiae* in a readily usable form. Genome Res. *12*, 1169–1173.

Imai, J., Toh-e, A., and Matsui, Y. (1996). Genetic analysis of the *Saccharomyces cerevisiae* RHO3 gene, encoding a rho-type small GTPase, provides evidence for a role in bud formation. Genetics *142*, 359–369.

Ito, H., Fukuda, Y., Murata, K., and Kimura, A. (1983). Transformation of intact yeast cells treated with alkali cations. J. Bacteriol. *153*, 163–168.

James, P., Halladay, J., and Craig, E. (1996). Genomic libraries and a host strain designed for highly efficient two-hybrid selection in yeast. Genetics *144*, 1425–1436.

Johnson, D.I. (1999). Cdc42: an essential Rho-type GTPase controlling eukaryotic cell polarity. Microbiol. Mol. Biol. Rev. *63*, 54–105.

Johnston, G.C., Prendergast, J.A., and Singer, R.A. (1991). The *Saccharomyces cerevisiae* MYO2 gene encodes an essential myosin for vectorial transport of vesicles. J. Cell Biol. *113*, 539–551.

Kagami, M., Toh-e, A., and Matsui, Y. (1997). SRO9, a multicopy suppressor of the bud growth defect in the *Saccharomyces cerevisiae rho3*-deficient cells, shows strong genetic interactions with tropomyosin genes, suggesting its role in organization of the actin cytoskeleton. Genetics *147*, 1003–1016.

Kagami, M., Toh-e, A., and Matsui, Y. (1998). Sro7p, a *Saccharomyces cerevisiae* counterpart of the tumor suppressor l(2)gl protein, is related to myosins in function. Genetics *149*, 1717–1727.

Kaiser, C., Gimeno, R., and Shaywitz, D. (1996). Protein secretion, membrane biogenesis, and endocytosis. In: The Molecular and Cellular Biology of the Yeast *Saccharomyces*, ed. J. Pringle, J. Broach, and E. Jones, Cold Spring Harbor, NY: Cold Spring Harbor, 91–228.

Karpova, T.S., McNally, J.G., Moltz, S.L., and Cooper, J.A. (1998). Assembly and function of the actin cytoskeleton of yeast: relationships between cables and patches. J. Cell Biol. *142*, 1501–1517.

Kroschewski, R., Hall, A., and Mellman, I. (1999). Cdc42 controls secretory and endocytic transport to the basolateral plasma membrane of MDCK cells. Nature Cell Biol. *1*, 8–13.

Kunkel, T.A., Roberts, J.D., and Zakour, R.A. (1987). Rapid and efficient site-specific mutagenesis without phenotypic selection. Methods Enzymol. *154*, 367–382.

Lehman, K., Rossi, G., Adamo, J.E., and Brennwald, P. (1999). Yeast homologs of tomosyn and *lethal giant larvae* function in exocytosis and are associated with the plasma membrane SNARE, Sec9. J. Cell Biol. 146, 125–140.

Lew, D.J., and Reed, S.I. (1995). Cell cycle control of morphogenesis in budding yeast. Curr. Opin. Genet. Dev. *5*, 17–23.

Madaule, P., Axel, R., and Myers, A.M. (1987). Characterization of two members of the rho gene family from the yeast *Saccharomyces cerevisiae*. Proc. Natl. Acad. Sci. USA *84*, 779–783.

Matsui, Y., and Toh-e, A. (1992a). Isolation and characterization of two novel ras superfamily genes in *Saccharomyces cerevisiae*. Gene *114*, 43–49.

Matsui, Y., and Toh-e, A. (1992b). Yeast *RHO3* and *RHO4* ras superfamily genes are necessary for bud growth, and their defect is suppressed by a high dose of bud formation genes CDC42 and BEM1. Mol. Cell. Biol. *12*, 5690–5699.

Novick, P., and Botstein, D. (1985). Phenotypic analysis of temperature-sensitive yeast actin mutants. Cell *40*, 405–416.

Novick, P., and Brennwald, P. (1993). Friends and family: the role of the Rab GTPases in vesicular traffic. Cell *75*, 597–601.

Pfeffer, S. (1999). Transport-vesicle targeting: tethers before SNAREs. Nature Cell Biol. *1*, 17–22.

Pringle, J.R., Bi, E., Harkins, H.A., Zahner, J.E., De Virgilio, C., Chant, J., Corrado, K., and Fares, H. (1995). Establishment of cell polarity in yeast. Cold Spring Harb. Symp. Quant. Biol. *60*, 729–744.

Protopopov, V., Govindan, B., Novick, P., and Gerst, J.E. (1993). Homologs of the synaptobrevin/VAMP family of synaptic vesicle proteins function on the late secretory pathway in *S. cerevisiae*. Cell *74*, 855–861.

Pruyne, D.W., Schott, D.H., and Bretscher, A. (1998). Tropomyosin-containing actin cables direct the Myo2p-dependent polarized delivery of secretory vesicles in budding yeast. J. Cell Biol. *143*, 1931–1945.

Richman, T., Sawyer, M., and Johnson, D. (1999). The Cdc42p GTPase is involved in a G2/M morphogenetic checkpoint regulating the apical-isotropic switch and nuclear division in yeast. J. Biol. Chem. *274*, 16861–16870.

Ridley, A.J. (1995). Rho-related proteins: actin cytoskeleton and cell cycle. Curr. Opin. Genet. Dev. *5*, 24–30.

Robinson, N.G., Guo, L., Imai, J., Toh-e, A., Matsui, Y., and Tamanoi, F. (1999). Rho3 of *Saccharomyces cerevisiae*, which regulates the actin cytoskeleton and exocytosis, is a GTPase which interacts with Myo2 and Exo70. Mol. Cell. Biol. *19*, 3580–3587.

Salminen, A., and Novick, P.J. (1987). A ras-like protein is required for a post-Golgi event in yeast secretion. Cell *49*, 527–538.

Tapon, N., and Hall, A. (1997). Rho, Rac and Cdc42 GTPases regulate the organization of the actin cytoskeleton. Curr. Opin. Cell Biol. *9*, 86–92.

TerBush, D.R., Maurice, T., Roth, D., and Novick, P. (1996). The exocyst is a multiprotein complex required for exocytosis in *Saccharomyces cerevisiae*. EMBO J. *15*, 6483–6494.

TerBush, D.R., and Novick, P. (1995). Sec6, Sec8, and Sec15 are components of a multisubunit complex which localizes to small bud tips in *Saccharomyces cerevisiae*. J. Cell Biol. *130*, 299–312.

Tkacz, J.S., and Lampen, J.O. (1973). Surface distribution of invertase on growing *Saccharomyces* cells. J. Bacteriol. *113*, 1073–1075.

Welch, M.D., Holtzman, D.A., and Drubin, D.G. (1994). The yeast actin cytoskeleton. Curr. Opin. Cell Biol. *6*, 110–119.